# MESOSCALE HEAT TRANSPORT OVER COMPLEX TERRAIN BY SLOPE WINDS – A CONCEPTUAL MODEL AND NUMERICAL SIMULATIONS ⋆

HEIKE NOPPEL⋆⋆ and FRANZ FIEDLER
*Institute for Meteorology and Climate Research, Universität Karlsruhe/Forschungszentrum Karlsruhe, Kaiserstr. 12, D-76128 Karlsruhe, Germany*

(Received in final form 6 December 2001)

**Abstract.** Vertical heat fluxes induced by mesoscale thermally driven circulations may contribute significantly to the subgrid-scale fluxes in large-scale models (e.g., general circulation models). However, they are not considered in these models yet. To gain insight into the importance and possible parameterisation of the mesoscale flux associated with slope winds, an analytical (conceptual) model is developed to describe the relationship between the mesoscale heat flux and atmospheric and land-surface characteristics. The analytical model allows us to evaluate the mesoscale flux induced by slope winds from only a few profile measurements within a domain. To validate the analytical model the resulting heat flux profiles are compared to profiles of highly resolved wind and temperature fields obtained by simulations with a mesoscale numerical model.

With no or moderate synoptic wind the mesoscale heat flux generated by the slope wind circulation may be as large as, or even larger than, the turbulent fluxes at the same height. At altitudes lower than the crest of the hills the mesoscale flux is always positive (upward). Generally it causes cooling within the boundary layer and heating above. Despite the simplifications made to derive the analytical model, it reproduces the profiles of the mesoscale flux quite well. According to the analytical model, the mesoscale heat flux is governed by the temperature deviation at the slope surface, the depth of the slope-wind layer, the large-scale lapse rate, and the wavelength of the topographical features.

**Keywords:** Analytical model, Heat flux, Mesoscale circulations, Numerical model, Slope winds.

## List of Symbols

| | |
|---|---|
| $D$ | large-scale domain |
| $H_{sw,M}$ | mesoscale flux of sensible heat induced by slope winds in domain M |
| $H_{sw,L}$ | mesoscale heat flux by slope winds averaged over half the valley width |
| $H_{\mathrm{tur}}$ | mean turbulent flux of sensible heat ($-\langle K_H \rangle \frac{\partial \langle \theta \rangle}{\partial z}$) |
| $K_H$ | eddy diffusivity for heat |
| $K_M$ | eddy diffusivity for momentum |

⋆ Dedicated to Professor Fritz Wippermann on the occasion of his 80th birthday.

⋆⋆ E-mail: heike.noppel@imk.fzk.de; f.fiedler@imk.fzk.de

*Boundary-Layer Meteorology* **104:** 73–97, 2002.

| | |
|---|---|
| $L$ | horizontal distance between valley axes and slope |
| $Pr$ | Prandtl number |
| $b$ | horizontal width of the slope wind layer |
| $d$ | mesoscale domain |
| $g$ | gravitational acceleration |
| $h$ | thickness of the slope wind layer perpendicular to the slope |
| $h_u$ | dynamical thickness of the slope wind layer |
| $h_\theta$ | thermal thickness of the slope wind layer |
| $l$ | measure for the depth of the slope wind layer |
| $n$ | coordinate perpendicular to the slope |
| $n_{\max}$ | height of slope wind maximum above ground |
| $n_V$ | number of valleys within a domain |
| $s$ | coordinate parallel to the slope |
| $u$ | horizontal wind component in $x$-direction |
| $u_s$ | wind component parallel to the slope |
| $\hat{u}$ | measure for the maximum slope wind speed |
| $w$ | vertical wind component |
| $z$ | vertical coordinate |
| $\alpha$ | slope angle |
| $\gamma$ | vertical gradient of $\theta_{VA}$ |
| $\lambda$ | topographical wavelength |
| $\phi$ | scalar variable |
| $\theta$ | potential temperature |
| $\theta_{VA}$ | potential temperature of the valley atmosphere |
| $\theta^*$ | temperature disturbance induced by the slope |
| $\hat{\theta}$ | $\theta^*(n = 0)$, temperature disturbance at the surface of the slope |
| $\Delta X$ | width of domain $M$ |
| $\langle\phi\rangle$ | average over a large-scale domain |
| $\langle\phi\rangle_M$ | average over a domain of GCM-grid size |
| $\langle\phi\rangle_L$ | average over half the valley width |
| $\langle\phi\rangle_{SWL}$ | horizontal average over the slope wind layer |
| $\overline{\phi}$ | average over a mesoscale domain |
| $\phi'$ | mesoscale deviation of $\phi$ |
| $\phi''$ | microscale deviation of $\phi$ |

## 1. Introduction

Atmospheric general circulation models (GCMs) have become an important tool to gain understanding of atmospheric processes and to forecast weather and climate. However, the spatial resolution of these models is limited by the available memory capacity and the required computing time. The latter is governed by the number of gridpoints and the maximum timestep for the integration, which decreases with increasing spatial resolution. Hence, the horizontal grid size of today's global climate models is about 200 km to 500 km (Cubasch, 1998), and that of global weather prediction models 50 km to 100 km (Majewski et al., 2001).

As several gridpoints are required to reproduce a meteorological process, these models simulate almost exclusively macroscale phenomena. Most mesoscale processes and microscale features, such as turbulence, are not resolved. Thermally induced circulations are primarily mesoscale subgrid processes and are not resolved appropriately in these models. These circulations arise from horizontal differential heating caused, for example, by land-sea transitions, sloping terrain, and differences in soil moisture or canopy. They can produce strong effects on the height of the convective boundary layer (Schädler, 1990), the turbulence structure and dispersion of trace gases within the boundary layer (Hadfield et al., 1992; Fiedler and Borell, 2000) and turbulent heat fluxes (Avissar and Chen, 1993) as well as the formation of clouds and precipitation (Anthes, 1994; Chen and Avissar, 1994). Theoretical and numerical investigations showed that these secondary circulation systems are connected to mesoscale transports of momentum, heat and mass that can be as large as, and larger than, turbulent fluxes, and can have a different vertical distribution than the turbulent fluxes averaged over the scale of a GCM grid increment (Pielke et al., 1991).

However, today's GCMs incorporate only microscale turbulence and disorganized convection as parameterised subscale processes. In doing this, a horizontally homogeneous surface is often presumed and parameterisation schemes based on observations in homogeneous terrain are employed. Effects of subscale inhomogeneities are mostly neglected. Some models allow for impacts of surface inhomogeneities on turbulent fluxes by using, for example, the mosaic method or effective land use and soil parameters (Fiedler and Panofsky, 1972; Baldauf, 1998). Since the accurate reproduction of atmospheric vertical transport of sensible heat, water vapour, and momentum as well as of the exchange between the surface and the atmosphere plays a crucial role in producing reliable model results, the development of enhanced parameterisation schemes for microscale processes in inhomogeneous terrain is an active area of current research.

Only in recent years have secondary circulations as subgrid processes and the vertical transport associated with them been investigated. Even these investigations have been confined almost exclusively to circulations driven by inhomogeneities over flat terrain.

However, nearly 70% of the earth's land surface consist of hills or mountains (Strobach, 1991) where horizontal differential heating takes place due to topography. The wind systems closely linked to topographical features include, apart from mountain valley winds, primarily slope winds.

Slope winds can be observed very frequently at all latitudes and in quite different relief. Consequently, it can be supposed that slope winds are able to produce a vertical heat flux that is significant not only locally but also on the long-term average over a large area. Although numerous single studies exist on this phenomenon (Atkinson, 1981; Egger, 1990; Whiteman, 1990; Barry, 1992; Noppel, 1999; Kossmann and Fiedler, 2000), there are few publications available dealing with the mesoscale heat flux associated with slope winds, and none discuss the impact of various parameters such as slope angle or atmospheric stability.

Therefore, this study aims to answer the following questions:

1. How large is the mesoscale heat flux caused by slope winds?
2. Which parameters affect this flux?

In the following sections the answers to these questions are obtained by conceptual considerations and by numerical simulations with a mesoscale model. Section 2 explains briefly the role of slope winds. In Section 3, we consider how mesoscale heat flux can be produced by slope wind circulations and develop a conceptual model to evaluate these heat fluxes. In Section 4, vertical profiles of the mesoscale heat flux are calculated using temperature and wind fields as simulated by a mesoscale numerical model. By means of these profiles we determine how well the conceptual model replicates the actual heat transport by slope winds. Finally, Section 5 summarizes the results and presents some conclusions.

## 2. Slope Winds

We use the following definition of 'slope wind': A slope wind is the wind that results from differential heating of the air near the slope and the air at the same altitude but farther away from the slope. The slope length is presumed to be several hundred metres to some kilometres. Slope winds are part of a thermally direct circulation in a vertical plane. Katabatic winds extending over a large area, like those occurring on the ice shields of Greenland and the Antarctic, as well as weak small-scale drainage flows, like those developing at hollows, will not be considered.

Figure 1 shows the conditions at a slope in a simplified form. A positive radiation budget at the surface heats the atmosphere from below during daytime. The air at the slope is warmer than the air in the valley. Due to buoyancy the warm air rises up the slope and an upslope flow forms. Subsidence in the centre of the valley follows from continuity. During nighttime, the temperature distribution and the circulation are reversed (Atkinson, 1981; Whiteman, 1990).

The slope wind system can be described as the small-scale end of a spectrum of thermally direct circulations that acts to transmit the sensible heat input along

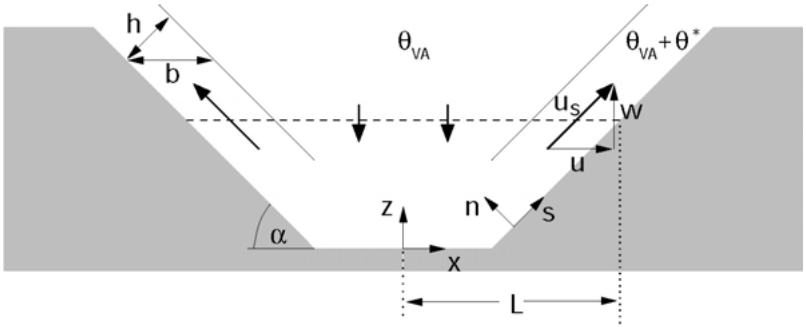


*Figure 1.* Schematic cross-section of a valley and slope-wind circulation during daytime. $h$, $b$: Height and width of the slope-wind layer; $\alpha$: slope angle; $u_s$: wind component parallel to the slope; $L$: valley width; $\theta_{VA}$: potential temperature of the valley atmosphere, $\theta^*$: temperature disturbance induced by the slope. It should be noticed that $L$ and $\theta_{VA}$ depend on $z$.

the slopes to the valley atmosphere (Vergeiner and Dreiseitl, 1987).The slope-wind circulation causes the breakup of the nocturnal stable boundary layer to procede in a different way than over flat terrain (Whiteman, 1982; Whiteman and McKee, 1982; Brehm, 1986; Freytag, 1987). Slope winds not only cause a redistribution of sensible heat but also of water vapour and air pollutants having their sources predominantly at the valley bottom (Barry, 1992; Kimura and Kuwagata, 1994; Vögtlin et al., 1996; Kossmann, 1998; Vogel et al., 1999).

The significance of the slope-wind system can be made clear by considering the resulting exchange of air and the heating due to compensating vertical motions. Consider a linear, symmetrical valley (see Figure 1) with a width of 10 km at mid-altitude of the ridges and a length $L_x$. The mean height of the right and left margin is assumed to be 800 m. From this a valley volume of $V = L_x \times A$, $A = 8\times10^6$ m$^2$ follows. On the slopes at both sides of the valley a slope-wind layer of 200 m should have evolved with a mean slope wind speed of 1 m s$^{-1}$. Hence, the total volume flux at the two slopes amounts to $\dot{V} = L_x \times 400$ m$^2$ s$^{-1}$. This means that in only $2\times10^4$ s – about 5.5 h – the total air volume of the valley is turned over by the slope winds. If the flow is non-divergent in the along-valley direction, the outflow of the slope winds will have to be compensated by a downward movement in the valley atmosphere. At mid-altitude of the ridges, the air has to subside with a velocity of about 0.04 m s$^{-1}$. Assuming a typical vertical gradient of potential temperature of 0.003 K m$^{-1}$ at this height, this subsidence produces a heating rate of $12\times10^{-5}$ K s$^{-1}$ (0.432 K h$^{-1}$), merely due to vertical advection of temperature. During the early morning this heating rate caused by subsidence may be supposed to represent the mean conditions in the valley. To achieve the same mean temperature increase of the valley atmosphere via vertical turbulent heat flux convergence, a source of turbulent heat flux at the valley bottom of more than 100 W m$^{-2}$ would be required.

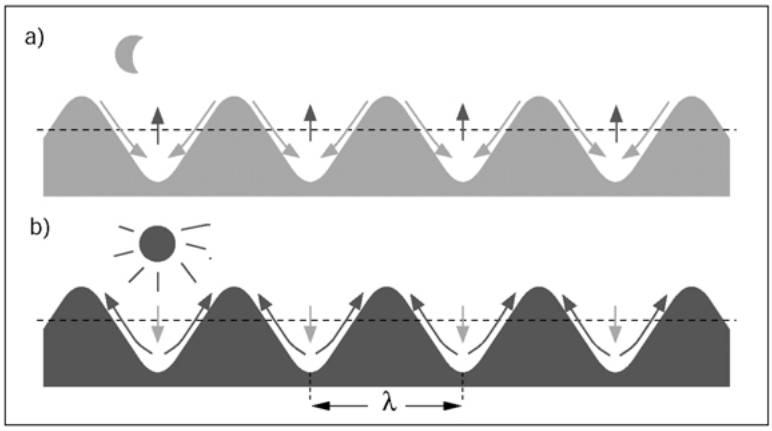


*Figure 2.* Heat transport by slope-wind circulation. (a) Situation at nighttime: Downward flow of relatively cool air in the slope-wind layer, rising of warm air near the centre of the valley. (b) Daytime situation: Upward flow of relatively warm air in the slope-wind layer, subsiding cold air near the centre of the valley. In both cases, an upward net heat transport through the layer depicted by the dashed line results.

## 3. Vertical Heat Transport Induced by Slope Winds

A large number of investigations have greatly extended our knowledge of the impact of various parameters, such as stability of the valley atmosphere and slope angle, on the slope wind. But the influence of these parameters on the mesocale flux induced by the slope winds is still unknown. Therefore, this section begins with some elementary thoughts on mesoscale fluxes and then continues to develop a concept for evaluating mesoscale heat flux and its dependence on the shape of orography and on atmospheric stratification.

Figure 2 depicts the situation during night and day in hilly terrain. At night the slope and the adjacent air cool. The cool air moves down the slope within the slope wind layer; in the valley atmosphere relatively warm air rises. During daytime the situation is reversed; the temperature of the slope and of the slope-wind layer increases strongly as insolation is converted to sensible heat flux at the ground. The warm air in the slope-wind layer rises and the cooler air in the valley atmosphere subsides. In both cases, heat is transferred upward through the layer depicted by the dashed line, i.e., the slope-wind circulation induces a positive mesoscale heat flux for both upslope wind and downslope wind.

### 3.1. Basic principles

Within a mesoscale domain $d$ a variable $\phi$ can be partitioned into a resolved part $\overline{\phi}$ and a subgrid-scale turbulent part $\phi''$, giving

$$\phi = \overline{\phi} + \phi''. \tag{1}$$

Several domains $d$ with a typical width of about 200 m to 2 km form a large-scale domain $D$ with a horizontal extent of about 20 km to 200 km. Consequently, a mean variable at the mesoscale resolution ($d$) can be written as the sum of a mesoscale perturbation $\phi'$ and a large-scale mean variable $\langle\phi\rangle$ defined as the average over the domain $D$

$$\langle\phi\rangle = \frac{1}{A(D)} \int_{A(D)} \overline{\phi}\, \mathrm{d}A. \tag{2}$$

Hence, we have

$$\overline{\phi} = \langle\phi\rangle + \phi' \tag{3}$$

and consequently

$$\phi = \langle\phi\rangle + \phi' + \phi''. \tag{4}$$

By decomposing vertical velocity $w$ and potential temperature $\theta$ in this way, the vertical kinematic heat flux can be expressed as

$$\begin{aligned} w\theta &= \langle w\rangle\langle\theta\rangle + \langle w\rangle\theta' + \langle w\rangle\theta'' + w'\langle\theta\rangle + w'\theta' \\ &+ w'\theta'' + w''\langle\theta\rangle + w''\theta' + w''\theta''. \end{aligned} \tag{5}$$

When averaged over $d$, noting that $\overline{\langle\phi\rangle} = \langle\phi\rangle$, $\overline{\phi'} = \phi'$, and $\overline{\phi''} = 0$, terms three, six, seven, and eight on the right-hand side vanish and we obtain

$$\overline{w\theta} = \langle w\rangle\langle\theta\rangle + \langle w\rangle\overline{\theta'} + \overline{w'}\langle\theta\rangle + \overline{w'\theta'} + \overline{w''\theta''}. \tag{6}$$

Further averaged over $D$, we obtain

$$\langle w\theta\rangle = \langle w\rangle\langle\theta\rangle + \langle w'\theta'\rangle + \langle w''\theta''\rangle, \tag{7}$$

where $\langle w'\theta'\rangle = \langle\overline{w'\theta'}\rangle$ and $\langle w''\theta''\rangle = \langle\overline{w''\theta''}\rangle$. If there are no other mesoscale processes besides slope winds, the mesoscale flux induced by the slope wind, $H_{sw}$, is $H_{sw} = \langle w'\theta'\rangle$. However, to quantify $\langle w'\theta'\rangle$ high spatial resolution information on the wind and temperature field in the domain is necessary. These data are, unfortunately, not available in most cases.

Generally, two issues arise when studying heat transport by slope winds:

(A) The determination of $H_{sw}$ from profile measurements at a few sites within the domain;

(B) the complexity of the slope wind system: various parameters and quantities affect the system and most of them interact with each other, so that even by mesoscale modelling the impact of single parameters may not be investigated.

A solution for both problems is provided by the following concept.

### 3.2. Net heat transport by slope-wind circulation in a valley and a grid element

To determine the mesoscale temperature flux $H_{sw}$ induced by a slope-wind circulation averaged over a valley ($H_{sw,L}$), some simplifications can be made at the outset. This includes the reduction of the dimensions of the problem by restricting the considerations on a valley cross-section as depicted in Figure 1 and assuming that variations along the valley's longitudinal axis can be neglected. Conditions are assumed to be symmetrical along this axis, so that it is sufficient to investigate only one half of the valley.

We then partition $\overline{\theta}$ into the potential temperature of the valley atmosphere, $\theta_{VA}$, which is not directly affected by the slope, and the disturbance impressed by the slope, $\theta^*$

$$\theta = \theta_{VA} + \theta^* + \theta''. \tag{8}$$

The vertical velocity is written as $w = \langle w \rangle + w' + w'' = \overline{w} + w''$. Applying these decompositions gives

$$w\theta = \overline{w}\theta_{VA} + \overline{w}\theta^* + \overline{w}\theta'' + w''\theta_{VA} + w''\theta^* + w''\theta''. \tag{9}$$

When averaged over a mesoscale domain $d$, the third, fourth, and fifth terms of the right-hand side of this equation cancel, giving

$$\overline{w\theta} = \overline{w}\theta_{VA} + \overline{w}\theta^* + \overline{w''\theta''}, \tag{10}$$

noting that $\overline{\theta_{VA}} = \theta_{VA}$ and $\overline{\theta^*} = \theta^*$.

As before we further average over a large-scale domain $D$, which now equals half the valley, giving

$$\langle w\theta \rangle_L = \langle \overline{w}\theta_{VA} \rangle_L + \langle \overline{w}\theta^* \rangle_L + \langle w''\theta'' \rangle_L. \tag{11}$$

Index $L$ at the brackets indicates an average over half the valley width. This average may be expressed as the weighted sum of the slope-wind layer average (indicated by the subscript *SWL*) and the valley atmosphere average (indicated by the subscript *VA*). Thus, for any quantity $\phi$

$$\langle \phi \rangle_L = \frac{L-b}{L} \langle \phi \rangle_{VA} + \frac{b}{L} \langle \phi \rangle_{SWL}, \tag{12}$$

where $b$ is the horizontal width of the slope-wind layer at a specific altitude $z$, and $L$ is the horizontal distance between the valley's longitudinal axis and the slope surface at the same altitude (see Figure 1).

Assuming horizontal homogeneity of $\theta_{VA}$, we have

$$\langle \overline{w}\theta_{VA}\rangle_L = \langle w\rangle_L \theta_{VA}, \tag{13}$$

noting that $\langle \theta_{VA}\rangle = \theta_{VA}$, and thus from Equation (11)

$$\langle w\theta\rangle_L = \langle w\rangle_L \theta_{VA} + \frac{L-b}{L}\langle \overline{w}\theta^*\rangle_{VA} + \frac{b}{L}\langle \overline{w}\theta^*\rangle_{SWL} + \langle w''\theta''\rangle_L. \tag{14}$$

Noting that $\theta^* = 0$ within the valley atmosphere, we have $\langle \overline{w}\theta^*\rangle_{VA} = 0$. To obtain the large-scale flux, $\theta_{VA}$ in the first term on the right-hand side has to be replaced by $\langle\theta\rangle_L$. Using Equation (8), noting that $\langle\theta''\rangle_L = 0$, and assuming horizontal homogeneity of $\theta_{VA}$, we have

$$\theta_{VA} = \langle\theta\rangle_L - \langle\theta^*\rangle_L = \langle\theta\rangle_L - \frac{b}{L}\langle\theta^*\rangle_{SWL} \tag{15}$$

and which reduces Equation (14) to

$$\langle w\theta\rangle_L = \underbrace{\langle w\rangle_L\langle\theta\rangle_L}_{\text{large-scale}} \underbrace{-\frac{b}{L}\langle w\rangle_L\langle\theta^*\rangle_{SWL} + \frac{b}{L}\langle \overline{w}\theta^*\rangle_{SWL}}_{\text{mesoscale}} + \underbrace{\langle w''\theta''\rangle_L}_{\text{turbulence}}. \tag{16}$$

The first and last term on the right-hand side of this equation correspond to the first and last term on the right-hand side of Equation (7). Consequently, the mesoscale heat flux induced by the slope-wind circulation on half-a-valley width is

$$H_{sw,L} = \frac{b}{L}\langle \overline{w}\theta^*\rangle_{SWL} - \frac{b}{L}\langle w\rangle_L\langle\theta^*\rangle_{SWL}. \tag{17}$$

In the two-dimensional case we have $\langle w\rangle_L = 0$ due to conservation of mass, and the second term on the right-hand side of Equation (17) vanishes.

If the topography in a large-scale domain $M$ of width $\Delta X$ (for example a GCM grid element) consists of a periodic sequence of $n_V$ identical valleys of wavelength $\lambda = \Delta X/n_V$, and if $\langle w\rangle_D = 0$, then the grid-element averaged heat flux by slope winds is given by

$$H_{sw,M} = \frac{n_V 2L H_{sw,L}}{\Delta X} = \frac{2L H_{sw,L}}{\lambda} = \frac{2b}{\lambda}\langle \overline{w}\theta^*\rangle_{SWL}, \tag{18}$$

where $\lambda$ is an external parameter, which has to be pre-set.

The mean over a large-scale domain, e.g., a grid element or a valley, can thus be reduced to the mean over the slope-wind layer, and hence $H_{sw,L}$ or $H_{sw,M}$ can be determined from profile measurements. Consequently, issue A is solved.

### 3.3. SUBSTITUTION OF $\langle \overline{w}\theta^* \rangle_{SWL}$ BY MEANS OF A SLOPE-WIND MODEL

Equation (18) can be used to solve issue B, if we know the parameters that govern the width $b$ or the height $h$ of the slope-wind layer, the temperature perturbation $\theta^*$, and the vertical wind $\overline{w}$ within the slope-wind layer. Several analytical slope-wind models are now available that describe the relationship between wind speed and temperature in the slope-wind layer and external parameters like atmospheric stability and slope angle (Brehm, 1986; Noppel, 1999).

One of the most prominent slope-wind models is that by Prandtl (Prandtl, 1942; Egger, 1990). Prandtl also decomposes potential temperature into $\theta_{VA}$ and $\theta^*$, which makes his model favourable for our purpose. The model provides $\theta^*$ and the velocity component parallel to the slope $\overline{u}_s$ as a function of the perpendicular distance from the slope $n$.

Prandtl assumes stationarity, a horizontally homogeneous valley atmosphere, a uniform, infinite slope, a motionless basic state, and constant diffusivities. $\overline{u}_s$ and $\theta^*$ follow from the equilibrium of buoyancy and friction, and from the equilibrium of temperature advection and microscale heat flux divergence,

$$\theta^*(n) = \hat{\theta} e^{-n/l} \cos(n/l) \tag{19}$$

$$\overline{u}_s(n) = \hat{\theta} \sqrt{\frac{g K_H}{\theta_{VA} \gamma K_M}} e^{-n/l} \sin(n/l) = \hat{u} e^{-n/l} \sin(n/l). \tag{20}$$

$K_H$ and $K_M$ are the eddy diffusivities for heat and momentum, $\alpha$ is the slope angle. The vertical gradient of potential temperature in the valley atmosphere $\gamma = \frac{\partial \theta_{VA}}{\partial z}$, is assumed to be constant. $\hat{\theta}$ is the temperature deviation at the ground, i.e., $\hat{\theta} = \theta^*(n = 0)$; $\hat{u} = \hat{\theta} \sqrt{\frac{g K_H}{\theta_{VA} \gamma K_M}}$ is a measure for the maximum wind speed. The measure for the depth of the slope-wind layer $l$ is given by

$$l = \left( \frac{4 \theta_{VA} K_H K_M}{g \gamma \sin^2 \alpha} \right)^{1/4}. \tag{21}$$

It should be noted that the model applies only for $\gamma > 0$ and $0° < \alpha < 90°$. Assuming a flow parallel to the slope within the slope-wind layer, $\overline{w}$ is given by $\overline{w} = \overline{u}_s \sin\alpha$.

Other investigations have shown that the slope flow can indeed be regarded as quasi stationary (Brehm, 1986) and that the advection due to changes in inclination can be neglected (Haiden, 1990).

Defant (1949) showed that Prandtl's solutions re-create observed profiles very well if the diffusivity or the characteristic length $l$ are fixed appropriately. The same conclusion is also drawn by Filliger et al. (1987). According to Ye et al. (1987) the assumption of $K_M$ being constant throughout the slope-wind layer leads to a wind maximum that is located too far from the ground, and that for rather shallow slopes

($\alpha = 0.6^o$) and slightly stable stratification the thickness of the slope-wind layer is overestimated.

The applicability of Prandtl's model for the conditions at a site at the edge of the Black Forest in south-west Germany was examined by Noppel (1999) with the help of tethered balloon soundings. As a rule, the height of the dynamic slope-wind layer proved to be over-estimated. The same is true for maximum wind speed during downslope flow. The differences between Prandtl's model and the measurements decrease with increasing stability of the valley atmosphere.

The vertical convective heat transfer within the slope-wind layer as calculated from Prandtl's profiles (Equations (19) and (20)) is

$$\begin{aligned}\langle \overline{w}\theta^* \rangle_{SWL} &= \frac{1}{h}\int_0^h \hat{\theta}\hat{u}\sin\alpha\, e^{-2n/l}\sin(n/l)\cos(n/l)\,dn \\ &= \frac{l\hat{\theta}\hat{u}\sin\alpha}{8h}\left\{-e^{-2h/l}\left(\sin(2h/l)+\cos(2h/l)\right)+1\right\}, \end{aligned} \tag{22}$$

where $h$, the height of the slope-wind layer, is not clearly defined. Generally two slope-layer depths can be distinguished: the dynamical thickness $h_u$ and the thermal thickness $h_\theta$. $h_u$ equals the value of $n$ where $u_s$ becomes zero and from Equation (20) we have

$$h_u = \pi l. \tag{23}$$

$h_\theta$ is the height where $\theta^*$ becomes zero, and results from Equation (19)

$$h_\theta = \frac{\pi l}{2}. \tag{24}$$

Using $h_u$ for $h$ in Equation (22) we obtain

$$\langle \overline{w}\theta^* \rangle_{SWL} = \frac{\hat{\theta}\hat{u}\sin\alpha}{8\pi}\left(1-e^{-2\pi}\right) \approx \frac{\hat{\theta}\hat{u}\sin\alpha}{8\pi}. \tag{25}$$

Inserting $h_\theta$ instead leads to

$$\langle \overline{w}\theta^* \rangle_{SWL} = \frac{\hat{\theta}\hat{u}\sin\alpha}{4\pi}\left(1-e^{-\pi}\right) \approx \frac{\hat{\theta}\hat{u}\sin\alpha}{4\pi}\,0.96. \tag{26}$$

Inserting Equation (25) in Equation (18), and noting that $b = \frac{h}{\sin\alpha} = \frac{\pi l}{\sin\alpha}$, we find that

$$H_{sw,M} = \frac{\hat{\theta}\hat{u}l}{4\lambda} = \frac{\hat{\theta}^2 l}{4\lambda}\sqrt{\frac{g}{\gamma\,\theta_{VA}\,Pr}}, \tag{27}$$

where the Prandtl number $Pr = \frac{K_H}{K_M}$ is used.

If $l$ is unknown, it can be estimated in different ways. According to Prandtl's model, $l$ may be expressed as $l = \frac{h_u}{\pi}$, $l = 2\frac{h_\theta}{\pi}$, or $l = 4\frac{n_{\max}}{\pi}$, where $n_{\max}$ is the height where $\overline{u}_s$ reaches its maximum. One shortcoming of Prandtl's model is the estimation of $h_u$ (Ye et al., 1987; Noppel, 1999). Due to this, the last two options are preferred. Using $h_\theta$ for $h$ instead of $h_u$ leads to an additional factor of 0.96 on the right-hand side of Equation (27).

According to Equation (27), the mesoscale heat flux by slope winds within a GCM grid element $H_{sw,M}$ is determined by the temperature deficit or surplus at the slope $\hat{\theta}$, the height of the slope-wind layer $l$, the vertical temperature gradient in the valley atmosphere $\gamma$, and the topographical wavelength $\lambda$. Other topographical parameters like valley width or slope angle do not appear in this relation, but they may affect $l$, $\hat{\theta}$, and $\gamma$.

Thus, issues A and B are solved, and the second of the objectives is attained. However, we have not yet shown, (a) if the concept as a whole is able to replicate reality despite all the simplifying assumptions, and (b) how much heat is actually transferred.

Noppel (1999) provided profiles of $\theta^*$ and $u_s$ from measurements at the western slope of the Black Forest in south-west Germany, and from these the horizontally averaged vertical heat flux in the adjoining Rhine valley can be calculated from Equation (17). At a height of 500 m above the valley bottom, and at a slope angle of 7.5°, a mean value of about 0.01 K m s$^{-1}$ is determined for $H_{sw,L}$, with a maximum of more than 0.02 K m s$^{-1}$ , which corresponds to about 24 W m$^{-2}$. A rough estimation of the turbulent flux at the same height suggests that the contribution of the slope-wind circulation to the total vertical transport of sensible heat is about 20% to 50% of that of the absolute mean turbulent flux at the same height during daytime. During nighttime the mesoscale flux may be even larger than the mean turbulent flux.

The daily variation of $H_{sw,L}$ derived from the measured profiles was compared with the one obtained by calculating $\langle w\theta^* \rangle_{SWL}$ with the help of Prandtl's model. Generally a good agreement results despite the nighttime values obtained by Prandtl's model being a little too high.

With the help of the measurements it can be shown that by inserting Prandtl's profiles the term $\frac{b}{L}\langle w\theta^* \rangle_{SWL}$ in Equation (17) can be determined. However, by means of measurements it is not possible to examine if the total concept is realistic. For that purpose it is necessary to determine if Equation (27) can replicate the actual net heat transport by the slope-wind circulation. For this, two- and three-dimensional high spatial and temporal resolution simulations were performed with the KAMM (**K**arlsruher **A**tmospheric **M**esoscale **M**odel) numerical model.

## 4. Results of Numerical Simulations

KAMM is a non-hydrostatic mesoscale numerical model. It consists of atmospheric and soil vegetation sub-models describing the interaction between soil, canopy and the overlying air, which are coupled by mass continuity and the surface energy balance. For a detailed description of the model see Dorwarth (1986), Schädler (1990), Adrian and Fiedler (1991), and Lenz (1996).

KAMM uses terrain following coordinates where the vertical grid size decreases from the top to the bottom of the model domain. A first-order closure is used for the turbulent fluxes, and the eddy diffusivities are derived using a mixing length as defined according to Blackadar (1962) and Fiedler and Panofsky (1972).

Seven model runs were carried out with an idealized, two-dimensional topography. In four simulations, the topography was changed from that of the reference run (see Figure 3). In one simulation, land use was changed from grass to forest, and in a further case, the initial background wind speed was changed from $0\,\mathrm{m\,s^{-1}}$ to $2\,\mathrm{m\,s^{-1}}$. The input parameters for KAMM and the different topographical characteristics are summarized in Tables I and II.

TABLE I

External parameters used in the numerical experiments.

| | |
|---|---|
| Day of year | 250 (7 Sept.) |
| Time of initialization | 2000 LST |
| Latitude | 49° |
| Number of gridpoints in x-direction (east–west) | 251 |
| Number of gridpoints in vertical direction | 85 |
| Height of model domain | 3600 m |
| Horizontal grid size | 300 m |
| Vertical grid size at the bottom | $\approx 1.4$ m |
| Soil class | Sandy loam |

### 4.1. Heat flux from mesocale covariance

The mesoscale model yields values for $\overline{w}$ and $\overline{\theta}$. The mesoscale disturbances, $w'$ and $\theta'$, were calculated from the simulated fields by

$$w' = \overline{w} - \langle w \rangle_M, \qquad \theta' = \overline{\theta} - \langle \theta \rangle_M, \tag{28}$$

where $\langle w \rangle_M = \langle \overline{w} \rangle_M$ and $\langle \theta \rangle_M = \langle \overline{\theta} \rangle_M$.

KAMM uses terrain following coordinates, but a GCM does not resolve the mesoscale topographic features. Thus, the spatial averaging $\langle\ \rangle_M$ and the evaluation of the mesoscale fluxes were performed on horizontal planes. Hence, the

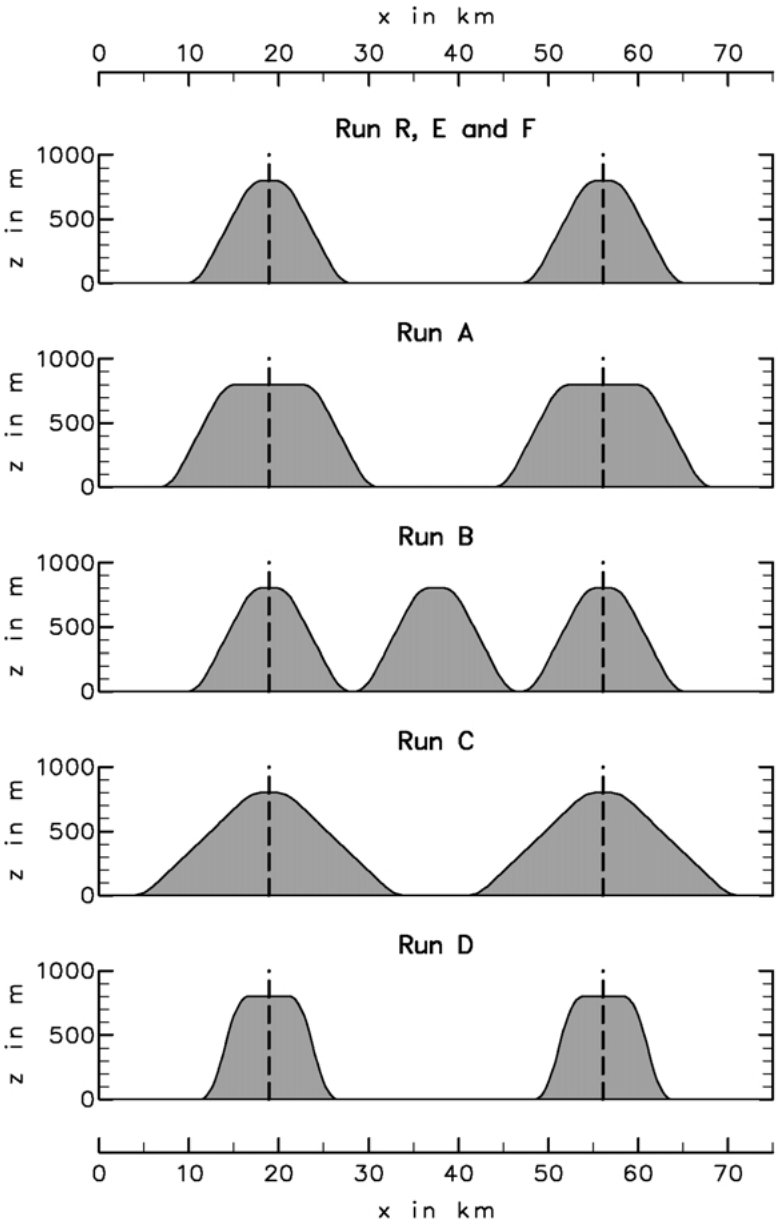


*Figure 3.* Topographies used for the simulations. The vertical dashed lines depict the left (western) and right (eastern) border of the domain over which the horizontal averaging was calculated.

TABLE II

Values of the parameters varied for the simulations: Slope angle, $\alpha$, valley width at mid-height of the valley $B_T$, topographical wavelength, $\lambda$, land use, and initial background wind speed $u_G$.

| Simulation | $\alpha$ (°) | $B_T$ (km) | $\lambda$ (km) | Land use | $u_G$ ($\mathrm{m\,s^{-1}}$) |
|---|---|---|---|---|---|
| R(eference) | 7.6 | 27.3 | 37.2 | grass | 0.0 |
| A | 7.6 | 21.3 | 37.2 | grass | 0.0 |
| B | 7.6 | 8.7 | 18.6 | grass | 0.0 |
| C | 3.8 | 21.3 | 37.2 | grass | 0.0 |
| D | 14.9 | 27.3 | 37.2 | grass | 0.0 |
| E | 7.6 | 27.3 | 37.2 | forest | 0.0 |
| F | 7.6 | 27.3 | 37.2 | grass | 2.0 |

simulated temperature and wind velocity had to be interpolated to the horizontal planes. Within the valley atmosphere, this was done by vertical linear interpolation. In the slope-wind layer $\overline{\theta}$ and $\overline{w}$ were interpolated parallel to the slope. Then the mesoscale flux was evaluated by $H_{sw,M} = \langle w'\theta' \rangle_M$.

Profiles of $\langle w'\theta' \rangle_M$ at different times (0400 LST and 1300 LST) are presented in Figure 4. In both cases $\langle w'\theta' \rangle_M$ vanishes at the valley bottom and at crest height (800 m). During nighttime the mesoscale heat flux depicts a maximum of $0.003\ \mathrm{K\,m\,s^{-1}}$ at an altitude of 100 m. Above a secondary maximum, it decreases linearly with height. During daytime the maximum is significantly higher up to about 400 m and reaches a value of about $0.02\ \mathrm{K\,m\,s^{-1}}$. Above the crests a second maximum occurs.

Changing the topography has little effect on the general shape of the profiles (Figures 5 and 6) and the impact on the absolute values is small as well. Setting the land use to 'forest' (simulation E) instead of 'grass' leads to a lower albedo and, due to higher roughness, to a stronger turbulent exchange between surface and atmosphere (Figure 8). This and the resulting higher thickness of the slope-wind layer are the main reasons for the mesoscale flux being much larger in the case of forest. Nevertheless, the shape of the profiles still remains similar.

Figures 4 to 6 also show the strong impact of the mesoscale lapse rate $\gamma = \frac{\partial \langle \theta \rangle}{\partial z}$ on $\langle w'\theta' \rangle$. During daytime the maximum of $\langle w'\theta' \rangle$ is always found near the upper edge of the boundary layer. As can be seen in Figure 7 this means that just where the mean turbulent heat flux, $H_{\mathrm{tur}}$, determined from $\langle \overline{K}_H \rangle_M$ and $\gamma$, is rather weak the mesoscale flux is strong. Figure 7 also shows that during nighttime the mesoscale flux is much stronger than the turbulent flux and is of opposite sign. As a consequence the total heat flux (turbulent plus mesoscale) is countergradient. During daytime the mesoscale and turbulent fluxes are both positive within the boundary layer, but $H_{\mathrm{tur}}$ decreases with height while $\langle w'\theta' \rangle$ increases. In the reference run

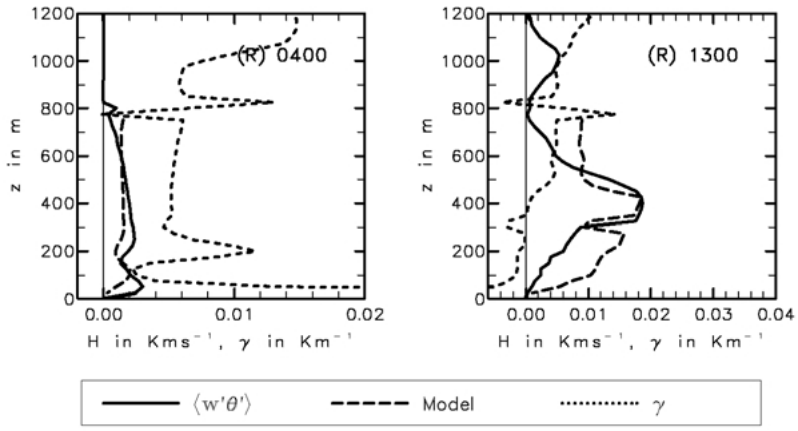


*Figure 4.* Profiles of mesoscale flux $\langle w'\theta' \rangle$ for the reference simulation (R) at 0400 and 1300 LST as computed from the covariances of the KAMM model results. The model-determined lapse rate is also shown, along with an alternate calculation of the mesoscale fluxes with the conceptual model ('Model').

$H_{\text{tur}}$ is nearly constant between 400 m and 700 m while the mesoscale and thus the total flux decreases and as a result heats the air above the boundary layer.

For a better assessment of the importance of $\langle w'\theta' \rangle_M$, Table III provides the mesoscale and mean turbulent heat flux, $H_{\text{tur}}$, as well as the temperature increase or decrease resulting from mesoscale and turbulent flux divergence determined from centred differences at different heights and times.

Compared to the sensible heat flux at the ground (Figure 8) the mesoscale heat flux induced by the slope-wind circulation seems rather small, but especially at night and higher above the valley bottom it cannot be neglected as compared to the turbulent flux. At night the mesoscale component contributes much more to the stabilization of the valley atmosphere than turbulence. During daytime the mesoscale transport counteracts the heating of the boundary layer while it causes heating above, and thus slows boundary-layer growth.

### 4.2. Mesoscale heat flux from the conceptual model

To evaluate the mesoscale heat flux $H_{sw,M}$ from the conceptual model, i.e., Equation (27), the following quantities have to be determined from KAMM simulations: the temperature deviation at the ground $\hat{\theta}$, the vertical temperature gradient within the valley atmosphere $\gamma$, the temperature of the valley atmosphere $\theta_{VA}$, and the characteristic slope-wind layer depth $l$. The topographical wavelength $\lambda$ is 18.6 km for simulation B and 37.2 km for all others. The Prandtl Number is set to $Pr = 1$.

The valley atmosphere temperature is approximated by the mean temperature, i.e., $\theta_{VA} \approx \langle \theta \rangle$, and $\gamma$ is estimated by $\gamma = \frac{\partial \langle \theta \rangle}{\partial z}$.To calculate $\hat{\theta}$ at the horizontal plane where the averaging is done the air temperature at the ground interpolated

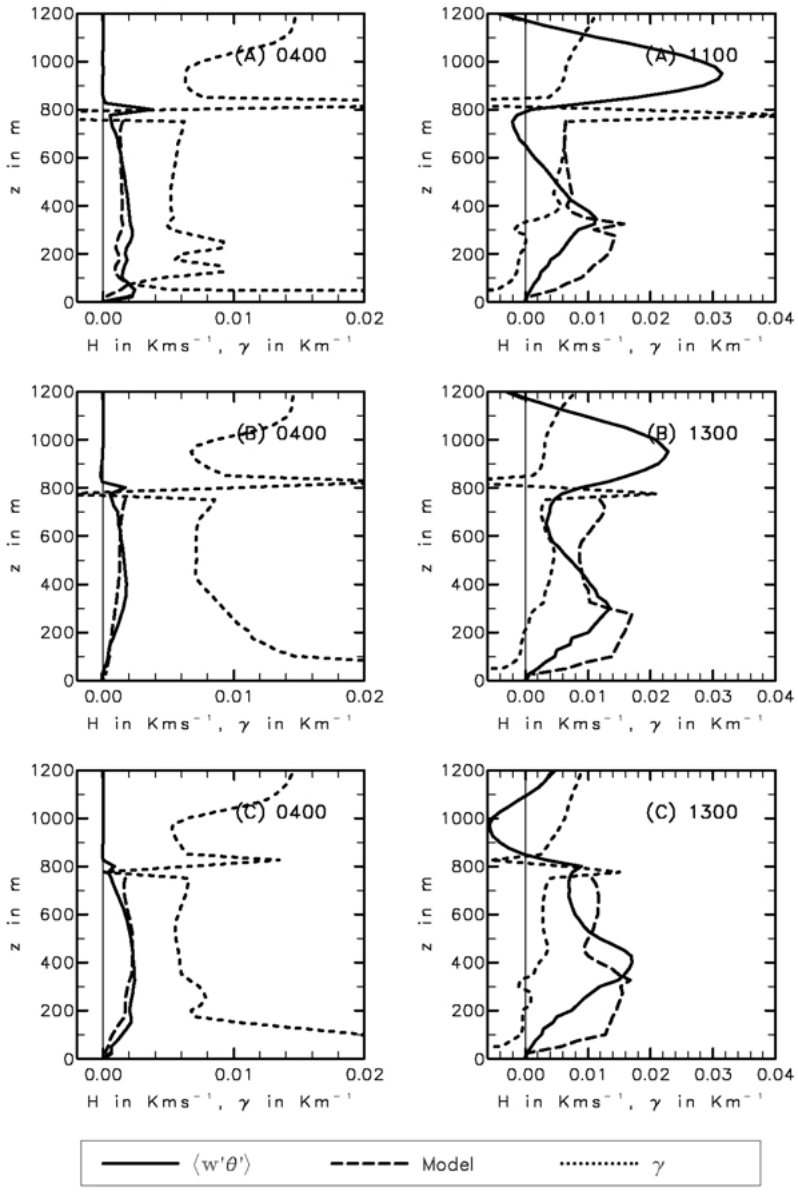


*Figure 5.* Same as Figure 4 for simulations A to C.

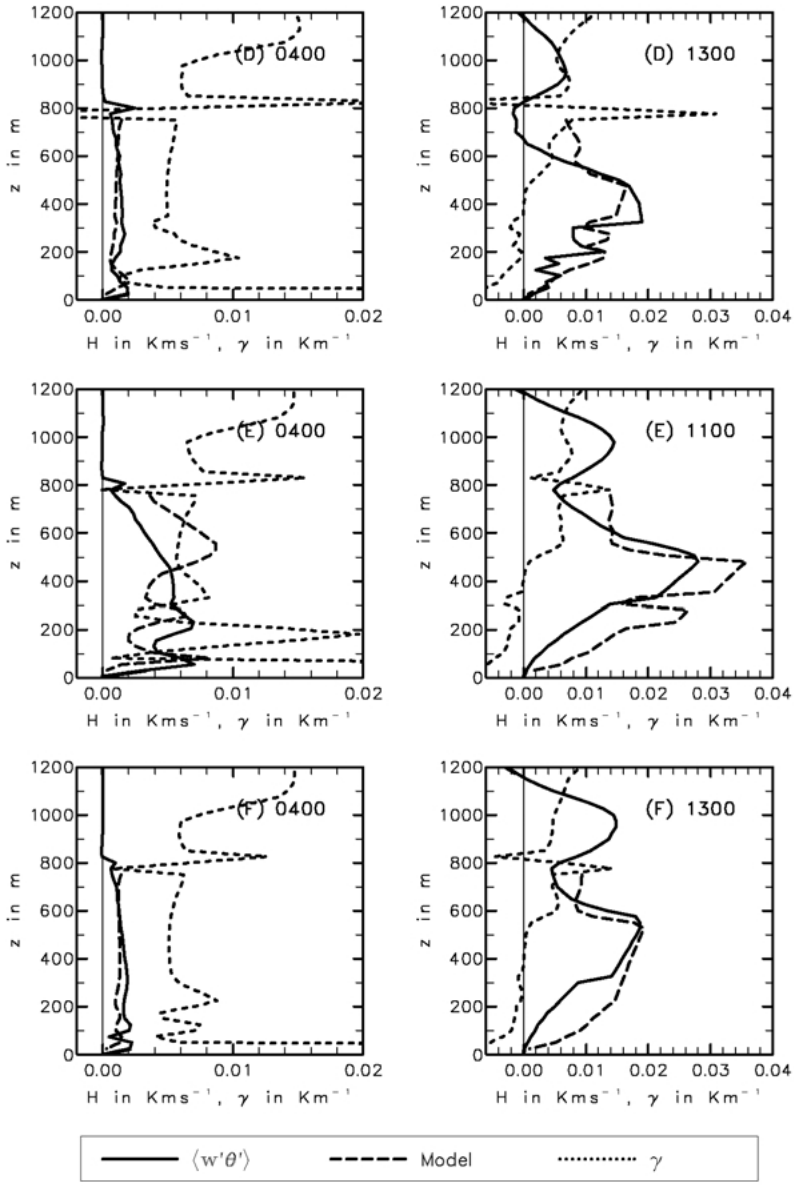


*Figure 6.* Same as Figure 4 for simulations D to F.

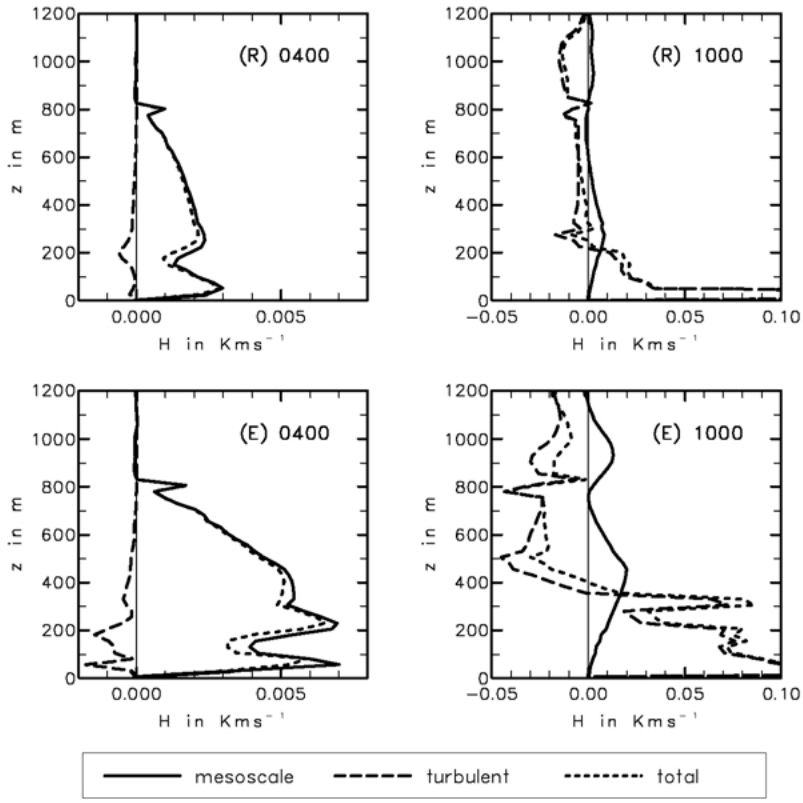


*Figure 7.* Profiles of mesoscale flux $\langle w'\theta' \rangle$ and mean turbulent flux $H_{\text{tur}}$ for simulations R and E at 0400 and 1000 LST.

parallel to slope and the deviation from $\theta_{VA}$ are calculated. Because insolation is different at the western and eastern slopes during daytime different values for $\hat{\theta}$ are obtained. To calculate $H_{sw,M}$ the average $\hat{\theta}$ was used. Figure 8 shows profiles of $\theta_{VA}$ and $\hat{\theta}$ for model runs R and E along with the profile of the diffusivity $K_H$ near the slope. During nighttime there is a significant correlation between $\theta_{VA}$ and $\hat{\theta}$ showing the influence of the conditions within the boundary layer on those in the slope-wind layer and vice versa. During daytime $\hat{\theta}$ increases with height within the boundary layer and is constant above. Consequently the shape of the profiles of the mesoscale heat flux may partly be attributed to the profiles of $\hat{\theta}$.

The simulated wind velocity fields showed that the height of the wind maximum above the ground $n_{\max}$ is very consistent. Therefore, $n_{\max}$, given in Table IV, was used to calculate $H_{sw,M}$, substituting $l$ from $l = \frac{4}{\pi} n_{\max}$. The fact that $n_{\max}$ is constant with height and much higher for grass than for forest agrees well with the profiles of $K_H$ near the slope (Figure 8).

TABLE III

Mesoscale, $\langle w'\theta' \rangle_M$, and turbulent heat flux, $H_{\text{tur}}$, as well as valley atmosphere heating (cooling) rate $\partial\theta_{VA}/\partial t$ resulting from flux divergences at different times of the day and different altitudes above the valley bottom.

| LST | height (m) | $\langle w'\theta' \rangle_M$ ($10^{-3}$ K m s$^{-1}$) | $H_{\text{tur}}$ ($10^{-3}$ K m s$^{-1}$) | $(\partial\theta_{VA}/\partial t)_{\text{meso}}$ (K h$^{-1}$) | $(\partial\theta_{VA}/\partial t)_{\text{tur}}$ (K h$^{-1}$) |
|---|---|---|---|---|---|
| | 600 | 1.33 | −0.03 | 0.02 | −0.00 |
| 0400 | 400 | 1.96 | −0.11 | 0.01 | −0.00 |
| | 200 | 1.86 | −0.60 | −0.09 | −0.01 |
| | 600 | 0.43 | −0.30 | 0.01 | 0.01 |
| 0700 | 400 | 0.76 | −0.19 | 0.00 | 0.00 |
| | 200 | 1.16 | −0.48 | −0.02 | 0.00 |
| | 600 | 0.09 | −5.32 | 0.06 | 0.01 |
| 1000 | 400 | 4.44 | −5.55 | 0.14 | −0.08 |
| | 200 | 6.10 | 11.22 | −0.25 | 2.08 |
| | 600 | 4.80 | −34.3 | 0.15 | −0.36 |
| 1300 | 400 | 18.62 | −18.78 | −0.00 | 2.15 |
| | 200 | 6.02 | 46.36 | −0.27 | 4.27 |

Figures 4 to 6 show that during daytime the stratification is often neutral or unstable in the lower part of the valley atmosphere. According to Equation (27) $H_{sw,M} \sim \gamma^{-1/2}$ is valid, where $\gamma$ is assumed positive. The simulations have shown, however, that even when $\gamma$ is negative slope winds can be maintained and hence transfer heat. However, as instability increases the slope-wind circulation becomes less significant and the mesoscale flux decreases. This means that $H_{sw,M}$ decreases with increasing absolute value of $\gamma$. For this reason, and as the true relationship between $H_{sw,M}$ and $\gamma$ is not known for $\gamma < 0$, we simply insert $|\gamma|$ instead of $\gamma$ in Equation (27).

TABLE IV

Height above ground of the wind speed maximum used to calculate $l$.

| Simulation | $n_{\max}$ (m) | |
|---|---|---|
| | Downslope wind | Upslope wind |
| R, A, C, D, F | 4.0 | 6.0 |
| B | 3.0 | 3.5 |
| E | 8.0 | 25.0 |

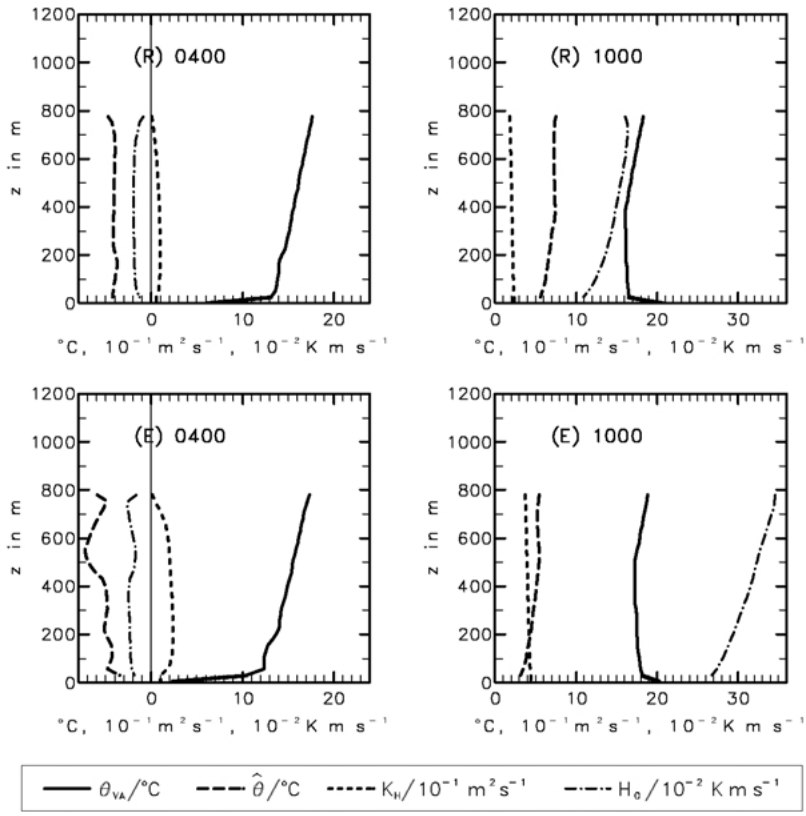


*Figure 8.* Profiles of $\theta_{VA}$, the temperature disturbance at the slope $\hat{\theta}$, the diffusivity for heat $K_H$ near the slope, and the sensible heat flux at the surface of the slope $H_0$ for simulations R and E at 0400 and 1000 LST. $\hat{\theta}$, $K_H$, and $H_0$ are averages of the values at the western and eastern slopes.

### 4.3. Comparison of results

The mesoscale heat flux profiles from the conceptual model are also shown in Figures 4 to 6. Considering the simplifications made to derive Equation (27), the assumption of a quite uniform $l$, and the somewhat arbitrary substitution of $\gamma$ by $|\gamma|$, the profiles compare quite well with $\langle w'\theta'\rangle_M$. For instance, the distinction between day and night and the position of the heat flux maximum are replicated correctly. Larger differences occur during daytime in the lower part of the valley and above the maximum. The first differences are attributed to $\gamma < 0$ in which case the use of Prandtl's model leads to some deviations. In most cases, the agreement is enhanced when $\gamma$ becomes positive. In the upper and lower regions of the slope some of the conceptual assumptions, such as homogeneity of the slope, are no longer satisfied. Additionally the conceptual model does not replicate the very strong return flow and the associated strong negative values of $w'\theta'$ occurring

in the KAMM simulations near the upper edge of the slope, which leads to an overestimation of the mean mesoscale flux.

## 5. Summary and Conclusions

Slope winds are a very common phenomenon in mountainous or hilly terrain and they are connected to the transport of mass and heat. The aim of this study was to investigate how large the mesoscale heat flux induced by slope wind is, what impact it may have, and which parameters affect this mesoscale flux.

The conceptual and numerical investigation of the net regional heat transport by slope-wind circulation leads to the following conclusions:

- The mesoscale vertical transport of sensible heat induced by slope-wind circulations has a considerable impact on the atmosphere even above the boundary-layer height. As a rule, the horizontally averaged mesoscale flux is always positive. Increasing with height within the boundary layer, and decreasing above, it produces cooling near the ground and heating higher up. During daytime, this opposes the effect of the turbulent flux. During nighttime, it leads to an additional stabilization, although the flux itself is positive.
- The mesoscale heat flux by slope winds may be as large as, or even larger than, the absolute value of the turbulent flux at the same height and should therefore be considered in GCMs.
- A simple conceptual model of the mesoscale heat flux has been developed in which the spatial mean over a valley or a GCM grid element, $\langle w'\theta' \rangle_M$, can be calculated as the mean over the slope wind layer $\langle \overline{w}\theta^* \rangle_{SWL}$ (Equation (18)). With this model the mesoscale heat flux in a mesoscale domain can be estimated from a few profile measurements in the valley and at the slope.
- Profiles of $\overline{w}$ and $\theta^*$ within the slope-wind layer can be input into our conceptual model from Prandtl's analytical slope-wind model, to calculate the heat flux by the slope-wind circulation in a specified domain using only a few parameters (Equation (27)).
- According to Equation (27), the mesoscale heat flux induced by slope winds is governed by the temperature deviation at the slope, the lapse rate in the valley atmosphere, the depth of the slope-wind layer, and the topographical wavelength. Further characteristics such as slope angle and roughness have an indirect impact.
- Results from observations and two-dimensional numerical simulations showed that equation (27) gives a useful estimate of the magnitude, the temporal variation, and the profiles of the mesoscale flux. Noppel (1999) shows that this is also valid for a real three-dimensional case.

Thus, the questions and issues mentioned in Sections 1 and 3.1 could be answered. Nevertheless, many other questions are still unsettled and new questions

arise, for example: how can $\hat{\theta}$, $l$ or $n_{\max}$ be determined in a large-scale model and what about separation of scales? The effects of along-valley winds on the mesoscale fluxes may also be important but were neglected in this study.

This study is only one first step but it has shown that the mesoscale fluxes induced by thermally forced circulations in mountainous terrain are significant. Therefore, more investigations on this subject are necessary. Future works should also investigate in a similar way the mesoscale transport of moisture and air pollutants by slope winds.

## Acknowledgements

Parts of this study were performed as part of the project 'Heat Moisture and Mass exchange Processes on a Regional Scale in a Non Homogenous Terrain' funded by the Commission of the European Communities (CEC).

The authors appreciate the critical comments on the manuscript made by Dr. Bernhard Vogel, Dr. Michael Baldauf and Dr. Meinolf Kossmann. Special thanks are also addressed to Prof. Charles D. Whiteman for his helpful comments and improvements of the English text.

This paper was written while the first author held a post-doctoral scholarship at the post-graduate course 'Natural Disasters' funded by the Deutsche Forschungsgemeinschaft (DFG).

## References

Adrian, G. and Fiedler, F.: 1991, 'Simulation of Unstationary Wind and Temperature Fields over Complex Terrain', *Beitr. Phys. Atmosph.* **64**, 27–48.

Anthes, R. A.: 1984, 'Enhancement of Convective Precipitation by Mesoscale (Subgrid-Scale) Variation in Vegetative Covering in Semiarid Regions', *J. Appl. Meteorol.* **23**, 541–554.

Atkinson, B. W.: 1981, *Meso-Scale Atmospheric Circulation*, Academic Press, London, 494 pp.

Avissar, R. and Chen, F.: 1993, 'Development and Analysis of Prognostic Equations for Mesoscale Kinetic Energy and Mesoscale (Subgrid-Scale) Fluxes for Large-Scale Atmospheric Models', *J. Atmos. Sci.* **50**, 3751–3774.

Baldauf, M.: 1998, *Die effektive Rauhigkeit über komplexem Gelände – ein störungstheoretischer Ansatz*, Wiss. Ber. Institut f. Meteorol. u. Klimaforschung, Karlsruhe, No. 24, 159 pp.

Barry, R. G.: 1992, *Mountain Weather and Climate*, Routledge, London, 401 pp.

Blackadar, A. K.: 1962, 'The Vertical Distribution of the Wind and Turbulent Exchange in a Neutral Atmosphere', *J. Geophys. Res.* **67**, 3095–3101.

Brehm, M.: 1986, *Experimentelle und numerische Untersuchungen der Hangwindschicht und ihrer Rolle bei der Erwärmung von Tälern*, Wissenschaftliche Mitteilung 54, Univ. München – Meteorologisches Institut.

Chen, F. and Avissar, R.: 1994, 'Impact of Land-Surface Moisture Variability on Local Shallow Convective Cumulus and Precipitation in Large-Scale Models', *J. Appl. Meteorol.* **33**, 1382–1402.

Cubasch, U.: 1998, 'Modellierung regionaler Klimaänderungen', in J. L. Lozàn, H. Grassl, and P. Hupfer (eds.), *Warnsignal Klima*, Wissenschaftliche Auswertungen, Hamburg.

Defant, F.: 1949, 'Zur Theorie der Hangwinde, nebst Bemerkungen zur Theorie der Berg – und Talwinde', *Arch. Meteorol. Geophys. Bioklim.* **A1**, 421–449.

Dorwarth, G.: 1986, *Numerische Berechnung des Druckwiderstandes typischer Geländeformen*, Wiss. Ber. Institut f. Meteorol. u. Klimaforschung, Karlsruhe, No. 6.

Egger, J.: 1990, 'Thermally Forced Flows: Theory', in W. Blumen (ed.), *Atmopheric Processes over Complex Terrain*, American Meteorological Society, Boston, pp. 43–57.

Fiedler, F. and Borell, P.: 2000, 'TRACT: Transport of Air Pollutants over Complex Terrain', in S. Larsen, F. Fiedler, and B. Borell (eds.), *Exchange and Transport of Air Pollutants over Complex Terrain and the Sea*, Springer-Verlag, Berlin, pp. 223–268.

Fiedler, F. and Panofsky, H. A.: 1972, 'The Geostrophic Drag Coefficient and the "Effective" Roughness Length', *Quart. J. Roy. Meteorol. Soc.* **98**, 213–220.

Filliger, F., Rickli, B., and Wanner, H.: 1987, 'Slope and Valley Wind Measurements and their Comparison with Ambient Winds and Stability', in *4th Conference on Mountain Meteorology*, Seattle, Washington, August 25–28, 1987, pp. 70–75.

Freytag, C.: 1987, 'Results from the MERKUR Experiment: Mass Budget and Vertical Motions in a Large Valley during Mountain and Valley Wind', *Meteorol. Atmos. Phys.* **37**, 129–140.

Hadfield, M. G., Cotton, W. R., and Pielke, R. A.: 1992, 'Large-Eddy-Simulations of the Thermally Forced Circulations in the Convective Boundary Layer. Part II: The Effect of Changes in Wavelength and Wind Speed', *Boundary-Layer Meteorol.* **58**, 307–327.

Haiden, T.: 1990, *Analytische Untersuchungen zur konvektiven Grenzschicht im Gebirge*, Ph.D. Dissertation, Formal – und Naturwiss. Fakultät der Universität Wien.

Kimura, F. and Kuwagata, T.: 1995, 'Horizontal Heat Fluxes over Complex Terrain Computed Using a Simple Mixed-Layer Model and a Numerical Model', *J. Appl. Meteorol.* **34**, 549–558.

Kossmann, M.: 1998, *Einfluss orographisch induzierter Transportprozesse auf die Struktur der atmosphärischen Grenzschicht und die Verteilung von Spurengasen*, Ph.D. Dissertation, Fakultät f. Physik der Universität Karlsruhe, 193 pp.

Kossmann, M. and Fiedler, F.: 2000, 'Diurnal Momentum Budget Analysis of Thermally Induced Slope Winds', *Meteorol. Atmos. Phys.* **75**, 195–216.

Lenz, C.-J.: 1996, *Energieumsetzung an der Erdoberfläche in gegliedertem Gelände*, Wiss. Ber. Institut f. Meteor. u. Klimaforschung, Karlsruhe, No. 19, 245 pp.

Majewski, D.; Liermann, D., Prohl, P., Ritter, B., Buchhold, M., Hanisch, T., Paul, G., Wergen, W., and Baumgartner, J.: 2001, 'The Global Isocahedral-Hexagonal Grid Point Model GME – Operational Version and High Resolution Test', *Workshop on Developments in Numerical Methods for Very High Resolution Global Models*, Reading, June 5–7 June, 2000, European Centre for Medium-Range Weather Forecasts, Reading.

Noppel, H.: 1999, *Untersuchung des vertikalen Wärmetransports durch die Hangwindzirkulation auf regionaler Skala*, Wiss. Ber. Institut f. Meteor. u. Klimaforschung, Karlsruhe, No. 25, 162 pp.

Pielke, R. A., Dalu, G. A., Snook, J. S., Lee, T. J., and Kittel, T. G.: 1991, 'Nonlinear Influence of Mesoscale Land Use on Weather and Climate', *J. Climate* **4**, 1053–1069.

Prandtl, L.: 1942, *Führer durch die Strömungslehre*, Vieweg und Sohn, Braunschweig.

Schädler, G.: 1990, 'Triggering of Atmospheric Circulations by Moisture Inhomogeneities', *Boundary-Layer Meteorol.* **51**, 1–29.

Strobach, K.: 1991, *Unser Planet Erde – Ursprung und Dynamik*, Gebr. Bornträger, Berlin.

Vergeiner, I. and Dreiseitl, E.: 1987, 'Valley Winds and Slope Winds – Observations and Elementary Thoughts', *Meteorol. Atmos. Phys.* **36**, 264–286.

Vogel, B., Fiedler, F., and Vogel, H.: 1999, 'Simulation von Perioden mit hohen Ozonkonzentrationen', in F. Gassmann et al. (eds.), *Luftqualität und Reginalklima*, REKLIP Final Report, Vol. 3, Editions Corpur, Strasbourg, pp. 133–170.

Vögtlin, R., Kossmann, M., Güsten, H., Heinrich, G., Fiedler, F., Corsmeier, U., and Klathoff, N.: 1996, 'Transport of Trace Gases from the Upper Rhine Valley to a Mountain Site in the Northern Black Forest', in P. M. Borell et al. (eds.), *Proceedings of the EUROTRAC Symposium '96*, Computational Mechanics Publications, Southampton, pp. 777–781.

Whiteman, C. D.: 1982, 'Breakup of Temperature Inversions in Deep Mountain Valleys: Part I. Observations', *J. Appl. Meteorol.* **21**, 270–289.

Whiteman, C. D.: 1990, 'Observations of Thermally Developed Wind Systems in Mountainous Terrain', in W. Blumen (ed.), *Atmopheric Processes over Complex Terrain*, American Meteorological Society, Boston, pp. 5–42.

Whiteman, C. D. and McKee, T. B., 1982: 'Breakup of Temperature Inversions in Deep Mountain Valleys: Part II: Thermodynamic Model', *J. Appl. Meteorol.* **21**, 290–302.

Ye, Z. J., Segal, M., and Pielke, R. A.: 1987, 'Effects of Atmospheric Thermal Stability and Slope Steepness on the Development of Daytime Induced Upslope Flow', *J. Atmos. Sci.* **44**, 3341–3354.